J Mater Sci: Mater Electron (2020) 31:21486–21501

Effect of different modifier oxides on the synthesis, structural, optical, and gamma/beta shielding properties of bismuth lead borate glasses doped with europium

R. Divina[1], K. A. Naseer[1], K. Marimuthu[1], Y. S. M. Alajerami[2,3], and M. S. Al-Buriahi[4,*]

[1] *Department of Physics, The Gandhigram Rural Institute (Deemed to be University), Gandhigram 624 302, India*
[2] *Physics and Astronomy, Science Faculty, Ohio University, Athens, USA*
[3] *Department of Medical Imaging, Al-Azhar University, Gaza Strip, Palestine*
[4] *Department of Physics, Sakarya University, Sakarya, Turkey*

Received: 11 July 2020
Accepted: 12 October 2020
Published online: 22 October 2020

ABSTRACT

A new set of bismuth lead borate glasses is synthesized using melt quenching technique with the chemical composition $39B_2O_3 + 30PbO + 20MO + 10Bi_2O_3 + 1Eu_2O_3$ (where M = K, Na, Ca, Sr and Ba). Lead based host matrix has been chosen since it acts as an effective material for radiation shielding applications. 30% of Lead oxide is used in every glass along with the varying modifier oxides and the comparative study is reported. The amorphous nature is confirmed via XRD analysis for the synthesized glasses. The physical and structural properties are calculated to get a clear idea about the potentiality of shielding that every glass can withstand. Mechanical strength of the glass is checked by calculating the Poisson's ratio, since breakage of glasses under stress conditions also need to be tested very much in the nuclear reactors for safety purposes. Optical studies are carried out through UV–Vis absorption spectra and the transitions between the energy levels of Eu^{3+} ions are reported. By using Tauc's plot direct and indirect band gap values are calculated along with Urbach energy values. Additionally, the radiation shielding properties of the synthesized glasses are also calculated by using both XCOM and ESTAR programs.

Address correspondence to E-mail: mohammed.al-buriahi@ogr.sakarya.edu.tr

https://doi.org/10.1007/s10854-020-04662-3

1 Introduction

Host of Bismuth Lead borate rich glasses with alkali and alkaline earth oxides like K_2O, Na_2O, CaO, SrO and BaO along with Europium oxide are synthesized for applications in radiation shielding. Radiation screening glasses are of high demand in the increasing industrial areas with nuclear power reactors as one of the quick surroundings [1]. Therefore utmost care is to be taken and it is a strict necessity to build screening wardrobes which is essential for the survival of human kind without any dreadful diseases like cancer. Glasses with neutron absorbing materials have high responsibility in providing shielding. Lead (Pb) with high molecular density has been used to effectively stop gamma and X-rays to escape from its coverage [2]. Thick block of Lead is normally used to store radiation waste or used as an apron for shielding purposes yet, taking this technique to the next level, lead based glasses are marvelous substitute for shielding purposes around the nuclear reactor. In Hospitals, X-Ray shielding glasses are used for high energy radiation therapy oncology, these glasses are preferred since it has a clear view and protection against the radiation is the absolute priority in diagnostic and therapeutic procedures [3].

In the recent times, Kavaz et al. [4] analyzed on the radiation shielding properties of $BaO–Bi_2O_3–B_2O_3–xCeO_2$ glasses for various concentration of CeO_2 and found that the glass with highest cerium content possess highest value of μ/ρ and HVL and is best for shielding radiation. Laariedh et al. [5] investigated the radiation shielding properties on lead based borate glasses with different modifiers like Tungsten, Sodium and Magnesium oxides and identified that the glass with 50% of Pb content exhibit larger ability to screen gamma radiations. Kawa et al. [6] theoretically and experimentally validated the gamma shielding properties with a new series of bismuth borate glasses modified with Zinc and Magnesium oxides. They estimated the radiation protection efficiency (RPE) and mass attenuation coefficient values and concluded the fact that the glass with 10% of Bismuth content exhibit more protection against the radiation when compared with the glass with 60% of Bismuth. Much earlier in 2004, Singh et al. [7] made a comparative study on lead borate and bismuth lead borate glasses and concluded that bismuth can be substituted with lead to attain the radiation shielding behavior near to lead based glasses. Newly, Marzouk et al. [8] investigated on the new series of heavy metal oxides like SrO, CdO, BaO, PbO or Bi_2O_3 doped borate glasses and studied the before and after effects on radiation and reported that Bismuth borate glasses exhibit excellent shielding material against gamma radiation. Based on the above findings, the present composition of glasses is synthesized.

In the present work, Borate is chosen as a glass former because of its technical importance and the flexibility of B_2O_3 to accommodate additives which facilitate the modified glass to be used for several applications. Heavy metal oxides like PbO, Bi_2O_3 is added into the glass matrix so that they can act as a glass modifiers and they have lower melting temperature, higher stability with flexible optical properties and reduce the phonon energy of the host matrix [9, 10]. Heavy metals incorporated glasses can be used extensively for gamma shielding applications as it aids in absorbing most of the fast moving neutrons [11]. Europium plays the role of dopant ion since it possesses many optoelectronic applications. Interestingly, apart from the optoelectronic device applications, high density RE-doped heavy metal alkali borate glasses exhibit improved radiation shielding properties for radiation shielding windows [11–13]. A host of borate rich glass containing alkaline earth oxides along with PbO, Bi_2O_3, SrO, BaO, CaO as glass modifiers are optimistic materials for their probable applications in the fields of optical communications, laser hosts, optical filters, X- and γ-ray absorbers, photonic devices, and so forth [14–16].

In the present work, bismuth lead borate glasses doped with europium ions were fabricated and their physical, structural, optical and radiation shielding properties were investigated. X-Ray Diffraction analysis was used to examine the amorphous nature of the fabricated glasses. Density and refractive index measurements employing Archimedes principle and Abbe refractometer respectively. Bandgap studies were calculated using Tauc's plot. The radiation shielding features of the fabricated glasses were inspected over a wide range of energy up to 15 meV.

2 Experimental and computational techniques

To synthesize a new series of bismuth lead borate glasses doped with europium ions, high purity Sigma Aldrich chemicals are used. Synthesized glasses with

their codes and chemical composition are given below;

BPBKE: $39B_2O_3 + 30PbO + 20K_2O + 10Bi_2O_3 + 1Eu_2O_3$.

BPBNaE: $39B_2O_3 + 30PbO + 20Na_2O + 10Bi_2O_3 + 1Eu_2O_3$.

BPBCaE: $39B_2O_3 + 30PbO + 20CaO + 10Bi_2O_3 + 1Eu_2O_3$.

BPBSrE: $39B_2O_3 + 30PbO + 20SrO + 10Bi_2O_3 + 1Eu_2O_3$.

BPBBaE: $39B_2O_3 + 30PbO + 20BaO + 10Bi_2O_3 + 1Eu_2O_3$.

Also, the weight fractions of the elements of the prepared glasses are given in Table1. 15 gm batch chemicals for BPBCaE, BPBSrE, BPBBaE glasses are weighed and minced as a homogeneous mixture which is taken in a porcelain crucible and melted in a furnace for 1.5 h at 1000 °C while the other two glasses BPBNaE and BPBKE are melted at 1200 °C for 10 and 11.5 h respectively. The melt is poured onto a preheated brass plate which is kept in the annealing furnace at 330 °C and 400 °C for different melting temperatures. The glasses are annealed for 10 h in order to improve the mechanical stability and to withstand stress and strain [17]. The annealed glasses are further polished and used for optical studies. The XRD analysis is performed by utilizing JEOL 8030 X-ray diffractometer (between $20° \leq \theta \leq 80°$) [18]. The XRD pattern of the BPBSrE glass is given in Fig. 1. The elemental analysis of glasses using EDX investigations is shown in Fig. 2. The oxidation states of elements are found out using XPS characterization and the increase or decrease of binding energy value of each photoelectron peak can be related to change of atoms environment, oxidation state in the chemical bonds. The intensity of B1s photoelectron peak is observed at 189.7 eV corresponding to + 3 oxidation state for Boron which also nearly matches the literature value of 191.1 eV. This small shift of the peak

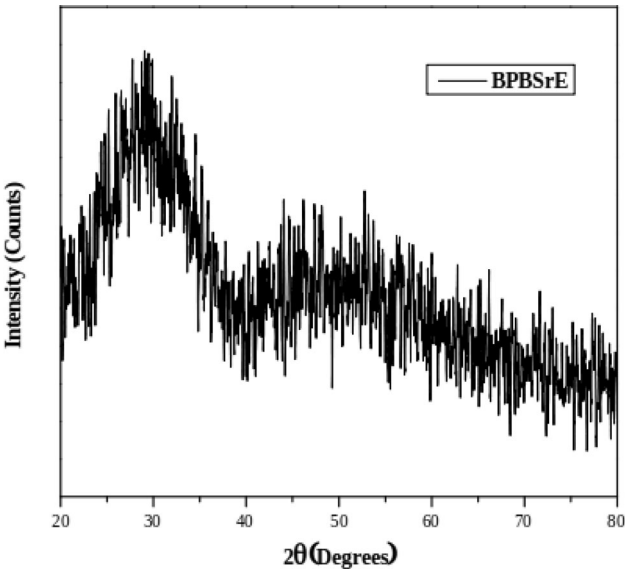

Fig. 1 XRD profile of the Eu^{3+} ions doped Bismuth Lead borate glass

positions can be explained due the addition of bismuth and lead into the chemical composition. The Bi4f photoelectron core level spectra point out a spin–orbit splitting of about 5.4 eV between $4f_{7/2}$ and $4f_{5/2}$ peaks. The peaks at 165.1 eV and 159.7 eV can be linked to the Bi^{3+} oxidation state of Bismuth in glass [19]. The Pb4f spectrum consists of two deconvoluted peaks such as $4f_{7/2}$ and $4f_{5/2}$ components positioned at 138.2 eV and 143.1 eV respectively and the oxidation state of Pb is + 2. In Eu3d spectra, the peak positions at 1135.2 eV and 1163.3 eV refers to Eu $3d_{5/2}$ and Eu $3d_{3/2}$ with the spin–orbit splitting of 28.1 eV which explains the Eu^{3+} oxidation state in glass. For Barium, there are two peaks $3d_{5/2}$ and $3d_{3/2}$ observed at 777.8 eV and 793.3 eV respectively with the splitting of 15.5 eV with the oxidation state of + 2 [20–22]. The appearance of an asymmetry in the O1s spectra is anticipated as it is well-known that the O1s peak in glasses arises from different oxygen binding sites. In

Table 1 The weight fraction and density of the new prepared glasses

Glass codes	Element (in wt.)										Density (g/cm^3)
	B	O	Eu	Pb	Bi	K	Na	Ca	Sr	Ba	
BPBKE	0.12112	0.33601	0.00863	0.27849	0.08969	0.1660					4.501
BPBNaE	0.12112	0.35367	0.00863	0.27849	0.08969		0.14837				4.597
BPBCaE	0.12112	0.35910	0.00863	0.27849	0.08969			0.14293			5.379
BPBSrE	0.12112	0.33292	0.00863	0.27849	0.08969				0.16911		5.982
BPBBaE	0.12112	0.32291	0.00863	0.27849	0.08969					0.1791	6.721

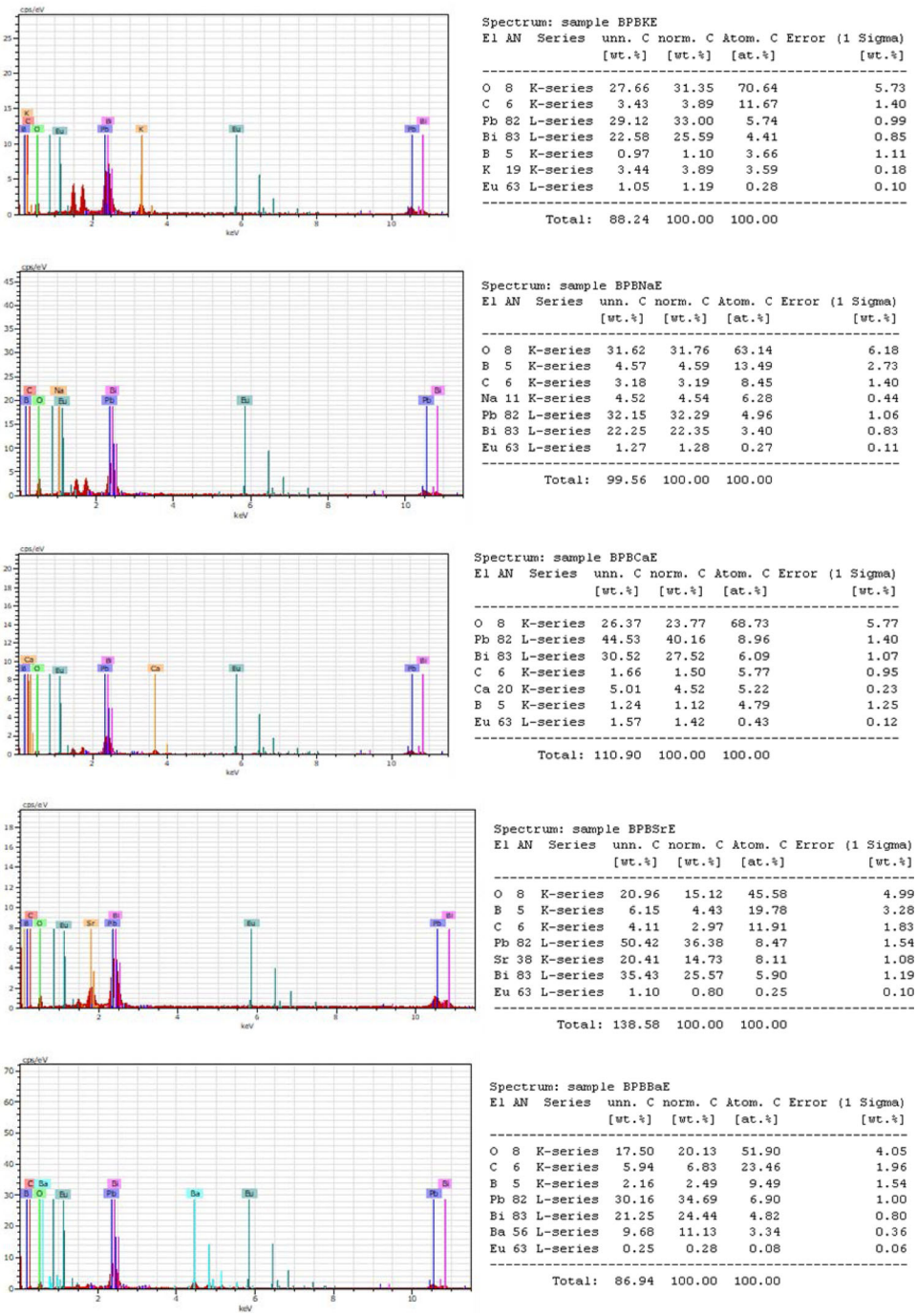

Spectrum: sample BPBKE

El	AN	Series	unn. C [wt.%]	norm. C [wt.%]	Atom. C [at.%]	Error (1 Sigma) [wt.%]
O	8	K-series	27.66	31.35	70.64	5.73
C	6	K-series	3.43	3.89	11.67	1.40
Pb	82	L-series	29.12	33.00	5.74	0.99
Bi	83	L-series	22.58	25.59	4.41	0.85
B	5	K-series	0.97	1.10	3.66	1.11
K	19	K-series	3.44	3.89	3.59	0.18
Eu	63	L-series	1.05	1.19	0.28	0.10
Total:			88.24	100.00	100.00	

Spectrum: sample BPBNaE

El	AN	Series	unn. C [wt.%]	norm. C [wt.%]	Atom. C [at.%]	Error (1 Sigma) [wt.%]
O	8	K-series	31.62	31.76	63.14	6.18
B	5	K-series	4.57	4.59	13.49	2.73
C	6	K-series	3.18	3.19	8.45	1.40
Na	11	K-series	4.52	4.54	6.28	0.44
Pb	82	L-series	32.15	32.29	4.96	1.06
Bi	83	L-series	22.25	22.35	3.40	0.83
Eu	63	L-series	1.27	1.28	0.27	0.11
Total:			99.56	100.00	100.00	

Spectrum: sample BPBCaE

El	AN	Series	unn. C [wt.%]	norm. C [wt.%]	Atom. C [at.%]	Error (1 Sigma) [wt.%]
O	8	K-series	26.37	23.77	68.73	5.77
Pb	82	L-series	44.53	40.16	8.96	1.40
Bi	83	L-series	30.52	27.52	6.09	1.07
C	6	K-series	1.66	1.50	5.77	0.95
Ca	20	K-series	5.01	4.52	5.22	0.23
B	5	K-series	1.24	1.12	4.79	1.25
Eu	63	L-series	1.57	1.42	0.43	0.12
Total:			110.90	100.00	100.00	

Spectrum: sample BPBSrE

El	AN	Series	unn. C [wt.%]	norm. C [wt.%]	Atom. C [at.%]	Error (1 Sigma) [wt.%]
O	8	K-series	20.96	15.12	45.58	4.99
B	5	K-series	6.15	4.43	19.78	3.28
C	6	K-series	4.11	2.97	11.91	1.83
Pb	82	L-series	50.42	36.38	8.47	1.54
Sr	38	K-series	20.41	14.73	8.11	1.08
Bi	83	L-series	35.43	25.57	5.90	1.19
Eu	63	L-series	1.10	0.80	0.25	0.10
Total:			138.58	100.00	100.00	

Spectrum: sample BPBBaE

El	AN	Series	unn. C [wt.%]	norm. C [wt.%]	Atom. C [at.%]	Error (1 Sigma) [wt.%]
O	8	K-series	17.50	20.13	51.90	4.05
C	6	K-series	5.94	6.83	23.46	1.96
B	5	K-series	2.16	2.49	9.49	1.54
Pb	82	L-series	30.16	34.69	6.90	1.00
Bi	83	L-series	21.25	24.44	4.82	0.80
Ba	56	L-series	9.68	11.13	3.34	0.36
Eu	63	L-series	0.25	0.28	0.08	0.06
Total:			86.94	100.00	100.00	

Fig. 2 EDX spectrum of Eu^{3+} ions doped Bismuth Lead borate glasses

general, a higher energy contribution arises from the presence of bridging oxygen (BO) atoms and oxygen atoms bonded to higher electronegativity cations (like B–O–B) and the lower energy peak results from the contribution of oxygen ions linked to the cations with lower electronegativity (such as Bi–O–Bi) and non-bridging oxygen (NBO) atoms. Thus, the two deconvoluted peaks 528.9 eV and 531.3 eV are observed in the O1s spectra with the splitting of 2.4 eV [22]. XPS spectrum of individual elements and survey spectrum for BPBBaE glass is shown in Fig. 3.

The MAC (μ_m) of the current glasses was determined by using the online XCOM program for wide range energy of 0.01 to 10 meV [23]. Based on the MAC, a series of shielding properties such as LAC, MFP, Z_{eff} and N_{eff} are determined by using the formulae mentioned in the Table 2.

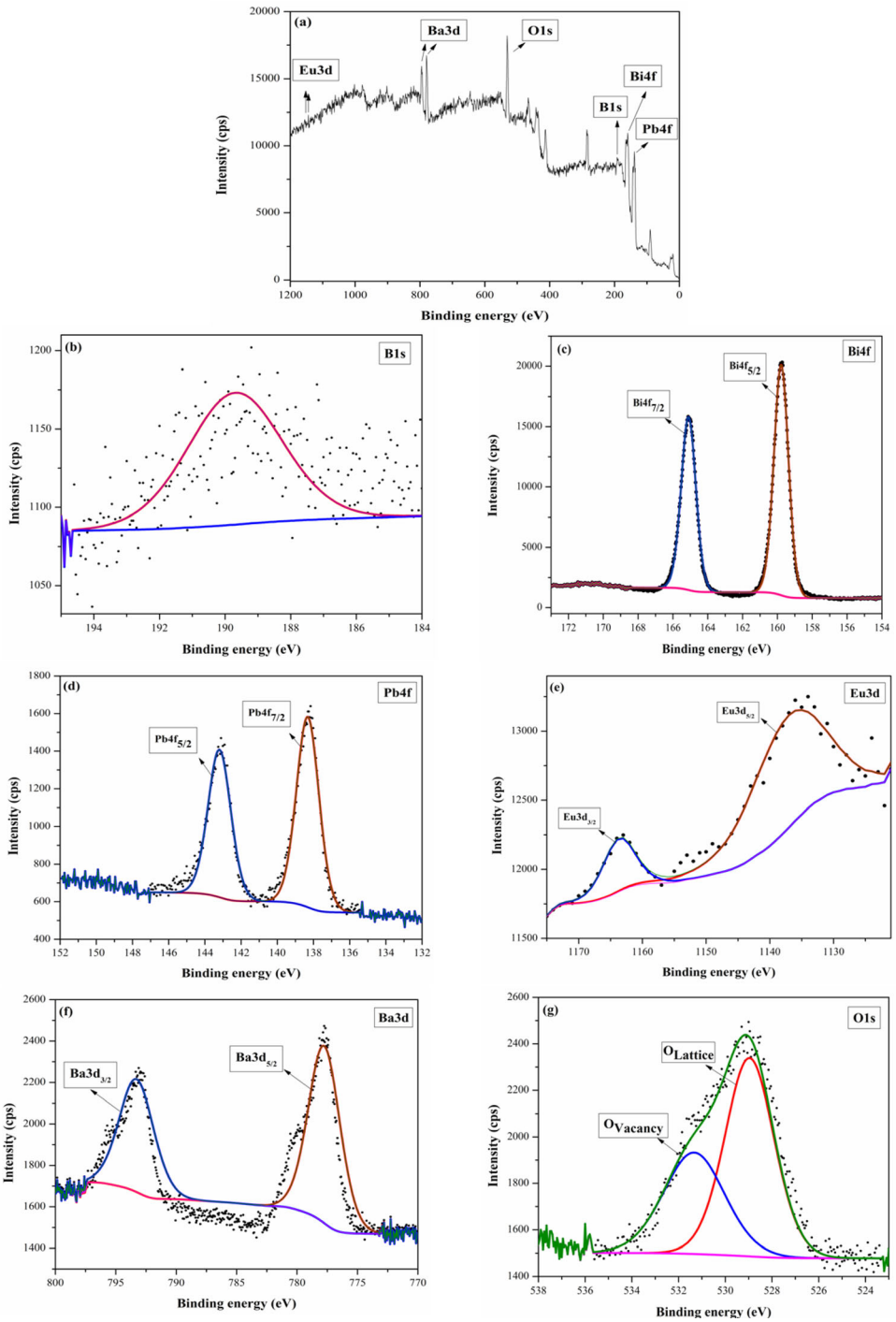

Fig. 3 XPS spectra of BPBBaE glass sample **a** Survey spectrum, **b** B1s, **c** Bi4f, **d** Pb4f, **e** Eu3d, **f** Ba3d and **g** O1s spectra

3 Results and discussions

3.1 Physical properties

In the case of applications which involve shielding of radiation, density and thickness are the important physical factors to be studied. Possession high density is one of the main characteristic features of all lead glasses. On the basis of effect of different modifiers, densities increases uniformly from 4.501 to 6.721 g/cc corresponding from BPBKE to BPBBaE glasses. The refractive index lies in the ranges 1.583–1.795 and all the glasses are polished to an equal thickness of 3 mm. Molar volume (V_m) and Average molecular weight (M_{av}) are calculated theoretically using the formulae referred from the

Table 2 Mathematical expressions for evaluating Radiation Shielding properties according to the Beer- Lambert's law [24]

Parameter	Formula	Symbols
LAC	LAC = MAC × ρ	ρ: density of glass
HVL	$HVL = \frac{0.693}{\mu}$	μ: linear attenuation coefficient = (density × μ/ρ)
MFP	$MFP = 1/\mu$	
Z_{eff}	$Z_{eff} = \frac{\sum_i f_i A_i (\frac{\mu}{\rho})_i}{\sum_j f_j \frac{A_j}{Z_j} (\frac{\mu}{\rho})_j}$	f_i is the fractional abundance of the element i, A_i is the atomic weight, and Z_i is the atomic number
N_{eff}	$Ne = (\frac{Z_{eff}}{M}) N_A \sum_i n_i$	M molecular weight ni number of formula units

literature [24, 25] and the observation shows the linear decrease of molar volume in relation with density and average molecular weight. Metallization criterion value (M) indicates the nature of solid as metals/non-metals. Heavy metal oxides doped glasses have R_m/V_m value ranging from 0.334 to 0.426 while the positive values of M indicates that the glasses come under the category of non-metals according to the theory by Dimtrov et al. [26]. All the physical properties of the Eu^{3+} ions doped bismuth lead borate glasses are listed in Table 3. The relationship among average molecular weight, density, and molar volume are pictorially represented in Fig. 4.

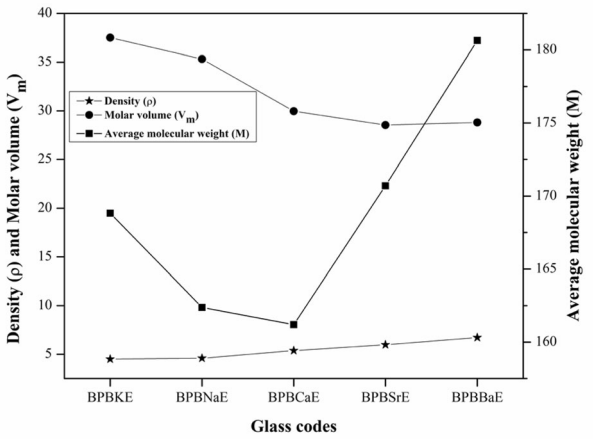

Fig. 4 Relationship among molar volume (V_m), average molecular weight (M) and density (ρ) with respect to the corresponding BPBxE glasses

3.2 Structural analysis

3.2.1 *Molar volume of oxygen (V_o), Oxygen packing density (OPD)*

As the glasses are mainly of oxides compounds there is an importance to check for the oxygen bonds as bridging or non-bridging since it connects the network as loosely or tightly packed structure. Molar volume and oxygen packing density reveals the structural changes occurred in every glass.

The theoretical formulae to calculate the above mentioned structural parameters are taken from the literature [27, 28] and presented below. For Molar volume of oxygen (V_o in cm^3/mol),

$$V_o = \frac{V_m}{\sum_i (\times n_o)_i}$$

For Oxygen Packing Density (OPD in mol/cm^3),

Table 3 Physical properties of Eu^{3+} ions doped Bismuth Lead borate glasses

Physical properties	BPBKE	BPBNaE	BPBCaE	BPBSrE	BPBBaE
Density ρ (g/cm^3)	4.501	4.597	5.379	5.982	6.721
Refractive index n_d (589.3 nm)	1.583	1.671	1.707	1.782	1.795
Average molecular weight M (g)	168.83	162.38	161.20	170.71	180.65
Molar volume V_m (cm^3/mol)	37.509	35.324	29.969	28.538	28.808
Optical dielectric constant (P	1.505	1.792	1.913	2.175	2.222
R_m/V_m	0.334	0.373	0.389	0.420	0.426
Metallization criterion (M)	0.665	0.626	0.610	0.579	0.574

$$\mathrm{OPD} = 1000 \times C \times \frac{\rho}{M}$$

As of Table 2, Molar volume of oxygen and oxygen packing density has values in the opposite trends which are the expected outcome. From BPBKE to BPBBaE glasses there is a linear decrease in V_o values from 13.946 to 10.028 cm^3/mol. On the other hand, OPD increases from 63.984 to 89.291 mol/cm^3. It is inferred from the results that, the increases in OPD is attributed to the increase in Bridging oxygens (BO) which makes the glass more connective [29]. The relation between Molar volume of oxygen and OPD is depicted in Fig. 5.

3.2.2 *Boron–Boron separation (< d_{B-B} >), Bond density (n_b)*

Boron–Boron separation is calculated to explore the arrangement of boron atoms as they are the basic building blocks in the present glasses. The alteration of boron atoms due to the introduction of different modifier cations can be known from this value. Based on the separation distance of glass former atoms and oxygen atoms, bond density is calculated theoretically using the formulae [30] and they are present below. For Boron-Boron separation (d_{B-B} in m),

$$\langle d_B - B \rangle = \left(\frac{V_m^B}{N_A}\right)^{1/3}$$

$$V_m^B = \frac{V_m}{2(1 - X_B)}$$

For Bond density (n_b in m),

$$n_b = \frac{N_A}{V_m} \sum_i (x n_c)_i = \frac{N_A}{V_m} n_{av}$$

From Table 4, it is observed that for the glasses from BPBKE to BPBCaE, the d_{B-B} value decreases and there is again an increase in for glasses BPBSrE and BPBBaE. This variation can be explained due to the non-linear changes in the average molecular weight and abrupt rise in density from 5.379 to 5.982 and 6.271 g/cc for BPBSrE and BPBBaE glasses respectively observed from Table 1. These changes affects the molar volume which in turn is responsible for the nearest neighboring co-ordination added bond density. Nearest neighbor co-ordination (n_{av}) have the same trend as of d_{B-B}. Moreover, the values of n_{av} lie approximately in the range in between 4.056 and 4.059, which is negligible. Therefore the occurrence of BO/NBO bonds can only be confirmed with bond density [30]. It is clear from the values of bond density that, there is a progressive rise in the number of bonds per unit volume from 6.52 to 9.12 ($\times 10^{28}$ m) for BPBKE to BPBBaE glasses respectively as of their densities. This is due to the increase in the number of bridging oxygens and the network becomes more rigid [31]. Relation prevailing among Boron-Boron separation and Bond density is pictorially reported in Fig. 6.

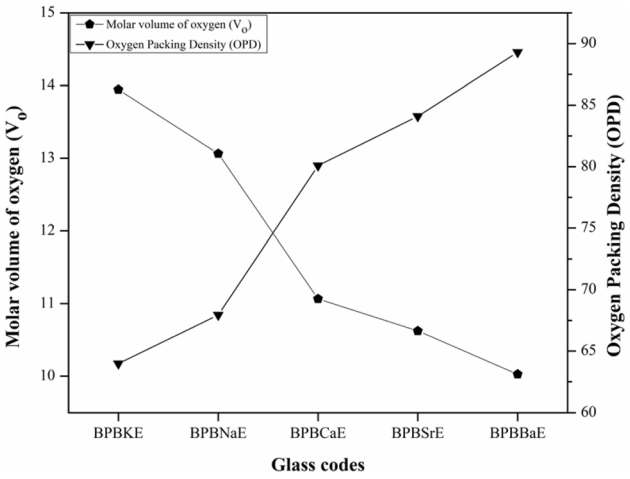

Fig. 5 Relationship between molar volume of oxygen (V_o) and Oxygen Packing Density (OPD) with respect to the corresponding BPBxE glasses

Table 4 The boron-boron separation ($d_{B-B} \times 10^{-10}$ m), molar volume of oxygen (V_o cm^3/mol), oxygen packing density (OPD mol/ cm^3), nearest neighbor coordination number (n_{av}), bond density ($n_b \times 10^{28}$ m^{-3}), optical basicity (Λ_{th}) of Eu^{3+} ions doped Bismuth Lead borate glasses

Parameters	BPBKE	BPBNaE	BPBCaE	BPBSrE	BPBBaE
d_{B-B}	4.4579	4.2461	3.9916	4.096	4.1244
V_o	13.946	13.064	11.066	10.624	10.028
OPD	63.984	67.944	80.084	84.101	89.291
n_{av}	4.056	4.053	4.053	4.056	4.059
n_b	6.52	6.92	8.16	8.57	9.12
μ_{cal}	0.214	0.223	0.256	0.277	0.298
Λ_{th} (n_d)	1.1347	1.0490	1.0075	1.046	1.0710

3.2.3 Optical basicity (Λ_{th}), ionicity (I_c%)

Optical basicity is an important parameter which determines the electron donating power of an oxygen atom in the oxide glass. The oxygen atoms behave as lewis bases since the oxygen atoms transfer part of its negative charge to cations and generally when basicity decreases there is a decrease in polarizability which further decreases the formation of NBO's [32]. In precise, there is increase in the formation of BO's. The ionic/covalent nature of the bonds in the glass system is checked using theoretical formulae [31]. For Optical Basicity,

$$\Lambda_{\text{th}} = \sum_{i}^{n} x_i \Lambda_i$$

For Ionic/covalent nature (in %),

$$C_{\text{iconic}}(I_c, \%) = \left[1 - \exp\{-0.25(\Delta\chi^2)\}\right] \times 100$$

$$C_{\text{covalent}}(C_c, \%) = \left[1 - \exp\{-0.25(\Delta\chi^2)\}\right] \times 100$$

As of Table 4, Optical basicity values decreases linearly from BPBKE to BPBCaE but for BPBSrE and BPBBaE glass there is a slight increase, the same kind of trend is observed while calculating the Bond density and Boron-Boron separation. These structural changes supports that there is an escalating connectivity in the glass network [31, 32]. From Table 5, Ionic character is found to be roughly between 74 and 79% while the covalency is much lesser around 20%. So, it is illustrated clearly that the network is more towards ionicity due to the addition of different modifiers even if the host is a lead based medium.

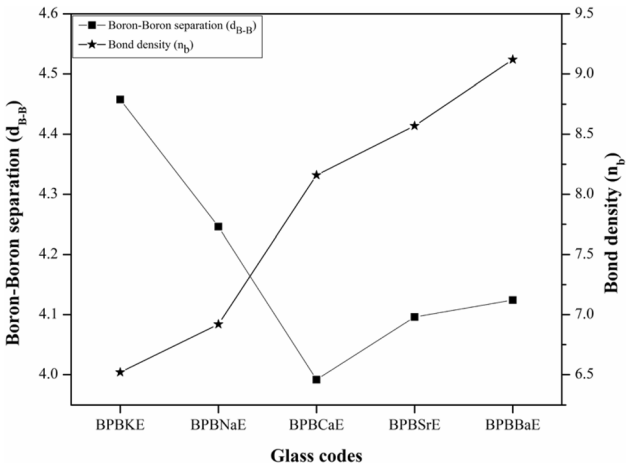

Fig. 6 Relationship between Boron-Boron separation $< d_{B\text{-}B} >$ and Bond density (n_b) with respect to the corresponding BPBxE glasses

3.2.4 Poisson's ratio (μ_{cal})

Poisson's ratio is one of the elastic properties which is used to determine the rigidity of the glass samples using the following theoretical formulae [33–35],

$$\mu_{\text{cal}} = 0.5 - \frac{1}{7.2V_t}$$

$$V_t = \frac{\rho_{\text{glass}}}{M_{\text{glass}}} \sum_i x_i V_i$$

$$V_i = \frac{4\pi N_A}{3}\left(nr_A^3 - mr_o^3\right)$$

Packing density V_t is used to calculate the value of poisson's ratio, ionic radii of cation and anion is represented as r_A and r_O. From the Table 4, μ_{cal} values are found to increase with increasing density. Reviews from different literature notify the fact that a high cross-link density has Poisson's ratio in the order of 0.1 to 0.2, while a low cross-link density has Poisson's ratio between 0.3 and 0.5. With this supposition, it can be concluded that the glass system has large cross-link density [33]. Thus, it can be said that the present glasses have high cross-link density.

3.3 Optical studies

3.3.1 UV–Vis-NIR studies

The optical absorption spectra of the Eu^{3+} ions doped Bismuth Lead borate glasses are recorded in the wavelength region 200–2500 nm and as a representative case UV–Vis-NIR absorption spectrum of the BPBKE glass is shown in Fig. 7. From the figure, it is observed that the absorption bands around 465, 2090 and 2203 nm corresponds to the transitions $^7F_0 \rightarrow {}^5D_2$, $^7F_0 \rightarrow {}^7F_6$ and $^7F_1 \rightarrow {}^7F_6$ respectively [36]. The $^7F_0 \rightarrow {}^5D_2$ transition is termed as hypersensitive transitions since it obeys the selection rules $\Delta J \leq 2$ and $\Delta L \leq 2$. No transitions could be observed below 400 nm due to the abrupt rise in the absorption edge as reported in Table 4 of the glass matrix [37].

3.3.2 Band gap studies with Tauc's plot

The absorption coefficient is calculated from the formula [37],

Table 5 Electro negativity (ΔX), ionic character factor (I_C,%) and covalent character factor (C_C, %) of Eu^{3+} ions doped Bismuth Lead borate glasses

Glass chemical compound	Electro negativity of elements	X_C	X_A	ΔX	I_C (%)	C_C (%)
B_2O_3	B (2.04), O (3.44)	4.08	10.32	6.24	99.99	0.01
PbO	Pb (1.87)	1.87	3.44	1.57	46.00	54.00
K_2O	K (0.82)	1.64	3.44	1.80	55.51	44.49
Na_2O	Na (0.93)	1.86	3.44	1.58	46.43	53.57
CaO	Ca (1.00)	1.00	3.44	2.44	77.43	22.57
SrO	Sr (0.95)	0.95	3.44	2.49	78.78	21.22
BaO	Ba (0.89)	0.89	3.44	2.55	80.32	19.68
Bi_2O_3	Bi (2.02)	4.04	10.32	6.28	99.99	0.01
Eu_2O_3	Eu (1.20)	2.40	10.32	7.92	100	0
$39B_2O_3 + 30PbO + 20K_2O + 10Bi_2O_3 + 1Eu_2O_3$					74.90	25.10
$39B_2O_3 + 30PbO + 20Na_2O + 10Bi_2O_3 + 1Eu_2O_3$					73.08	26.92
$39B_2O_3 + 30PbO + 20CaO + 10Bi_2O_3 + 1Eu_2O_3$					79.28	20.72
$39B_2O_3 + 30PbO + 20SrO + 10Bi_2O_3 + 1Eu_2O_3$					79.55	20.45
$39B_2O_3 + 30PbO + 20BaO + 10Bi_2O_3 + 1Eu_2O_3$					79.86	20.14

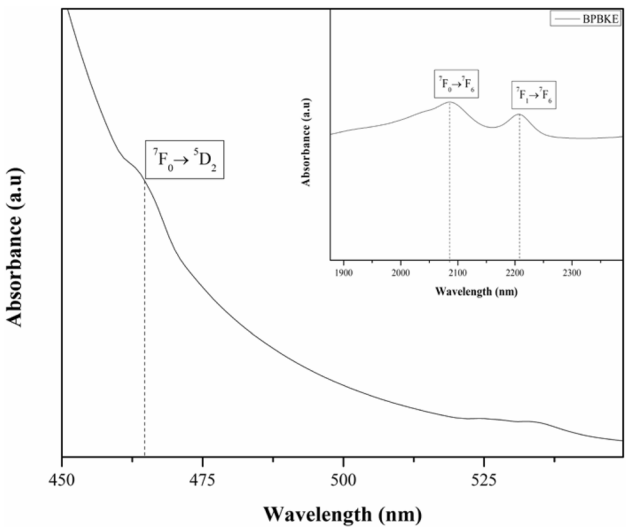

Fig. 7 UV–Vis absorption spectrum of the BPBKE glass [Inset shows the NIR region absorption spectrum of the BPBKE glass]

$$\alpha(v) = (1/d)\ln(I_o/I_t)$$

where d is the thickness of glass sample, I_o and I_t are the intensities of the incident and transmitted radiations respectively. Davis and Mott gave a relation that exist between the optical band gap, the absorption coefficient, and the same is given as,

$$\alpha h\nu = B(h\nu - E_{opt})^m$$

where h is the plank's constant, B is the band tailing parameter, E_{opt} is the optical band energy, and m denotes the index number as 1/2, 2 corresponding to direct and indirect allowed transitions. Figures 8 and 9 show the Tauc's plot for direct and indirect transitions and the transitions are extrapolated to X-axis to get the band gap values. It is observed from the Tauc's plot and Table 4 that the glasses have band gap lying in the range 2.565–2.741 eV and 2.313–2.515 eV for direct and indirect transitions respectively. The linear increase in the bandgap value from BPBKE to BPBBaE glass explains the formation of bridging oxygens in the glass network which makes the glass more rigid [38].

Urbach energy (ΔE) measures the disorderliness in the glass system; therefore much less the value of ΔE indicates the much less the number of defects in the glass. From Table 6, it is found that the values lie in between 0.257 and 0.459 eV. Therefore this indicates the much lower extension of tail width of localized states into the forbidden band gap.

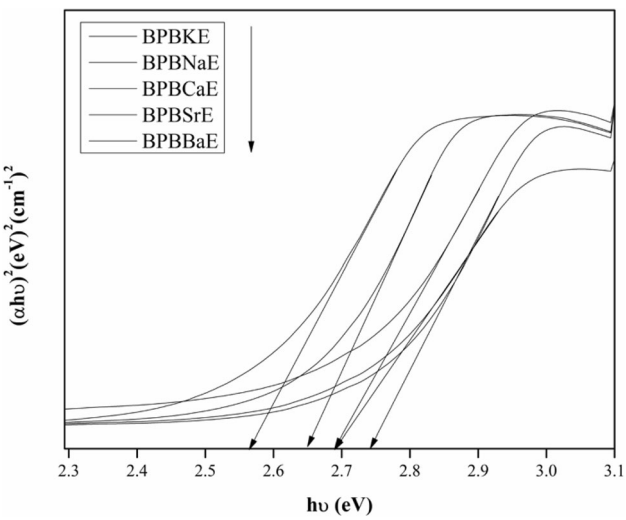

Fig. 8 Tauc's plot for the allowed direct transitions of Eu^{3+} ions doped Bismuth Lead borate glasses

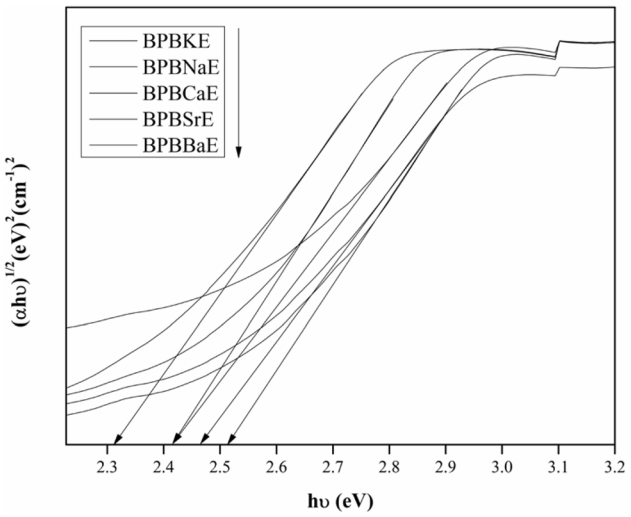

Fig. 9 Tauc's plot for the allowed indirect transitions of of Eu^{3+} ions doped Bismuth Lead borate glasses

3.4 Radiation shielding studies

The density of the prepared glasses and the weight fraction of the preceding materials are listed in Table 1. Except the value obtained at BPBKE, the density of the glasses was enhanced obviously by increasing of atomic number and to molecular weight of K_2O, Na_2O, CaO, SrO, and BaO. This trend is expected that the increment of these oxides be on the expanse of B_2O_3. The density of BPBKE was slightly less than BPBNaE, and this is because sodium is denser than potassium and there is a slightly increase in atomic size and atomic volume as we move from sodium to potassium.

Figure 10 shows the mass attenuation coefficient (μ_m) values of the prepared glasses, obtained by XCOM program between 0.01 and 10 meV [39]. In this figure, the enhancement of the μ_m values is consistent with increasing of glass density. Therefore, the glass with BaO (BPBBAE) owns the highest μ_m value, whereas that with K_2O (BPBKE) is the lowest, which is consistent at all energies. This behavior can be attributed to the higher effective atomic cross section of K_2O, NaO, CaO, SrO, and BaO than B_2O_3. The highest μ_m values for the glasses is found at 10 keV and equal to 81.123, 85.631, 88.316, 89.882 and 91.437 cm^2/g for BPBKE, BPBNaE, BPBCaE, BPBSrE and BPBBaE respectively. In addition, we reported discontinues in the values of the attenuation at 0.09 meV. These discontinues are related to the K-absorption edge of Pb. At 1.0 meV, the μ_m values for the prepared samples are respectively 0.064, 0.066, 0.069, 0.072 and 0.075 cm^2/g. This emphasizes that the calculated μ_m values improved by increasing of glass density. At low energy level (< 0.4 meV), the μ_m for all prepared glasses showed large values and become to decrease gradually with increasing of photon energy. The sudden increase at 0.1 meV is expected due to the K absorption edge of PbO. Sequentially, the values reduced with slower rate between 0.1 and 1.0 meV compared to that at low energy < 0.4 meV. Above 1.0 meV, the μ_m values were very low and become almost stationary. According to the energy of incident photon, three possible interactions are expected photoelectric absorption (PE), Compton scattering (CS) and pair production (PP) at low, intermediate and high energies, respectively. Consequently, the absorber will show high μ_m values at 0.8 to 0.1 meV due to the dominant of PE absorption, which has high effective cross section related to the incident energy and atomic number of absorber ($1/E^{3.5}$ and Z^4).Therefore, BPBBaE sample that has the highest atomic number (BaO) showed the highest μ_m and this energy level [40, 41]. At intermediate energy level, the cross section of Compton scattering varies with less effect of photon energy and atomic number of absorber $1/E$ and Z, respectively (compared with low energy level) [40–42].

The half value layer (HVL) is a term used in the radiation shielding aspect to determine the thickness of the absorber that can show that half of the incident

Table 6 The fundamental absorption edge (λ_{edge}), optical band gap (E_{opt}), band tailing parameter (B) corresponding to the direct (n = ½) and indirect (n = 2) allowed transitions and Urbach energy (ΔE) of Eu^{3+} ions doped Bismuth Lead borate glasses

Glass code	λ_{edge}	n = ½		n = 2		ΔE (eV)
		E_{opt} (eV)	B (cm^{-2} eV)^2	E_{opt} (eV)	B (cm^{-2} eV)$^{1/2}$	
BPBKE	444	2.565	520.88	2.313	4.62	0.275
BPBNaE	433	2.648	629.03	2.415	4.94	0.381
BPBCaE	419	2.689	695.13	2.418	5.17	0.416
BPBSrE	419	2.692	726.24	2.463	5.75	0.437
BPBBaE	417	2.741	787.53	2.515	6.06	0.459

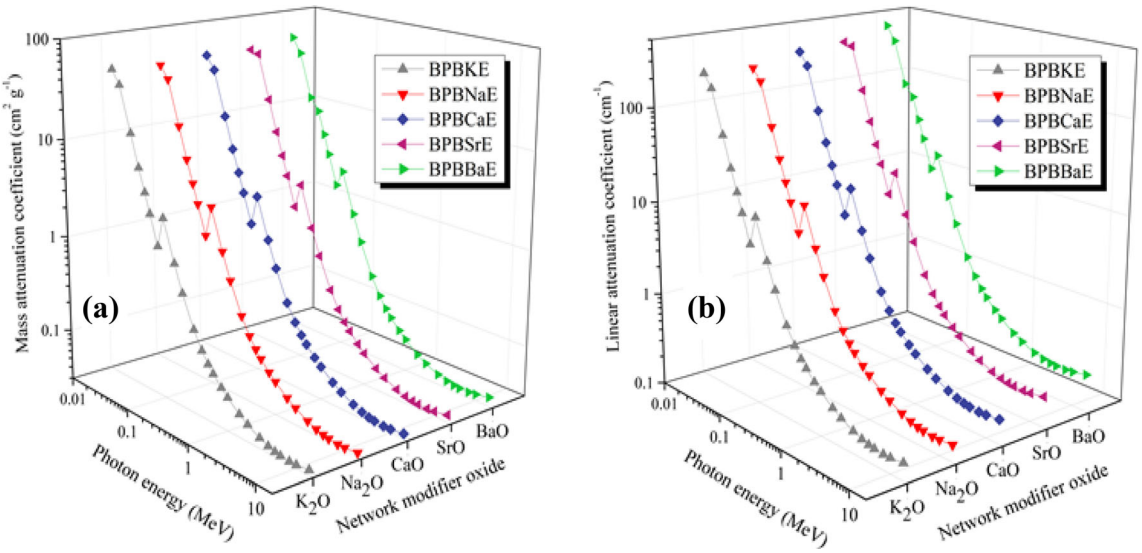

Fig. 10 Variation of **a** mass and **b** linear attenuation coefficient with photon energy for the new prepared glasses

radiation. In other term, it is important to get appropriate thickness to attenuate the intending radiation by the absorber intend to be used in the radiation facilities. This concept can be directly estimated from the μ_m values of the absorber as shown in Fig. 11. We revealed the HVLs of the prepared glasses at different energies (0.01 to 10 meV). The smallest HVL is achieved with BPBBaE glass. For example, at 0.1 meV the HVL is varied between 0.0711 cm (for BPBKE), 0.0691 cm (for BPBNaE), 0.0587 (for BPBCaE), 0.0505 (for BPBSrE) and 0.0404 (for BPBBaE). The maximum HVL for all glasses was reported at 10 meV (4.5482, 4.6071, 3.8028 and 2.7688 respectively) and this direct relation between incident energy and HVL thickness is expected. The BaO has higher density than that of B_2O_3, therefore has higher attenuation factor (the ability to attenuate of radiation beam per unit distance). Thus, the replacement of B_2O_3 by BaO increases the density in this work to 6.721 g/cm^3 (the highest glass density). The high density absorber can shield and attenuate more photons, so the HVL is small for the high density medium. Comparing the obtained HVL for BPBBaE with some standard shielding materials like (ordinary concrete, hematite-serpentine concrete, ILC: ilmenite-limonite concrete, BMC: basalt-magnetite concrete, IC: ilmenite concrete, SSC: steel-scrap concrete, SMC: steel-magnetite concrete [43]) at specific energy (for example 0.5 meV) got the lowest HVL (0.8852 cm).

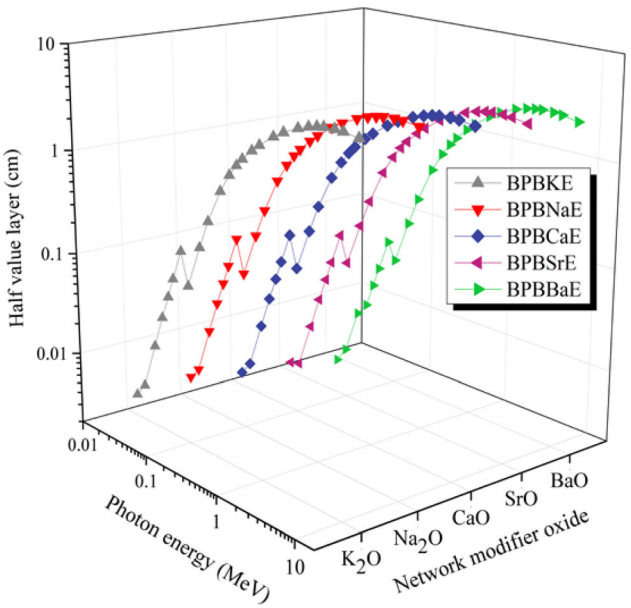

Fig. 11 Variation of the half value layer (HVL) with photon energy for new glass samples

Figure 12 illustrates the relation between incident photon energy and calculated MFP for the new glasses. At low energies, a gradual increase in MFP was observed with increasing of photon energy. Except of BPBSrE that showed gradual increase of MFP (maximum value at 10 meV), the maximum MFP values of other glasses were reported at ~ 8 meV then started to decrease with low rate (almost constant) at higher energies. This behavior may ascribe to the different possibilities of photon

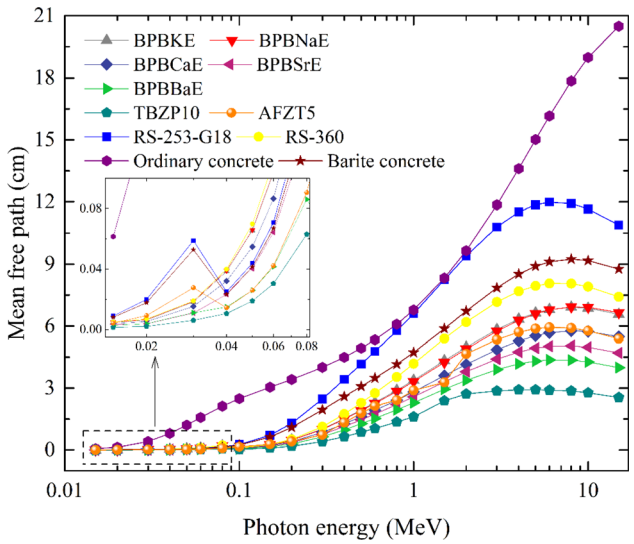

Fig. 12 Variation of the mean free path (MFP) with photon energy for new glasses compared with standard materials (TBZP10 [44], RS-253-G18 [45], RS-360 [46], Ordinary concrete [46], and Barite concrete [46])

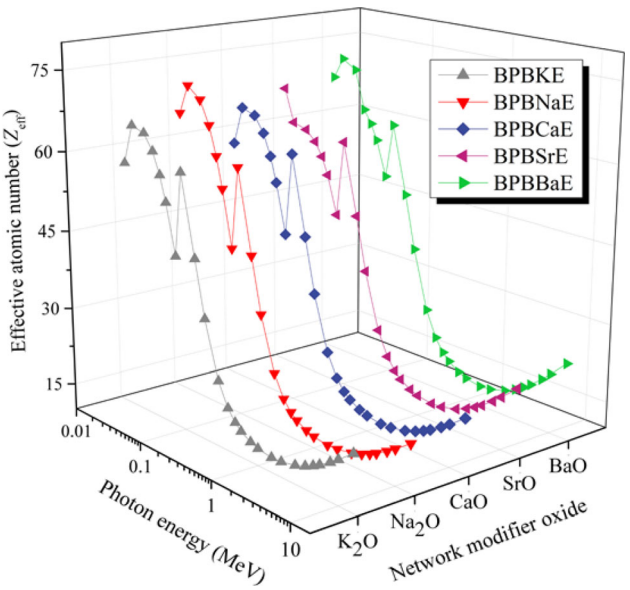

Fig. 13 Variation of the effective atomic number (Z_{eff}) with photon energy for new glasses

interaction with the glasses. Then the glass includes BaO content, exhibited the smallest MFP and it owns promising gamma shielding properties. In the new prepared glasses, the MFP achieved by BPBBaE is also favorable with that obtained by standard shielding glass and concrete materials like RS-253-G18, RS-360, ordinary concrete, and barite concrete and very close to that obtained by TBZP10.

The effective atomic number (Z_{eff}) profile for the new prepared glasses is similar to other borate based glasses reported recently by different groups [47–49]. As shown in Fig. 13, the Z_{eff} shows several trends with the energy and the maximum values for this parameter occur at the first several photon energies (firstly Z_{eff} is high and reaches maxima at 0.02 meV). The maximum values reported at 0.02 meV for all glasses are equal to 64.65, 70.54, 64.75, 60.23 and 71.47. The photoelectric effect explains that the high Z_{eff} at $E \leq 0.02$ meV illustrates the sharp reduction in the Z_{eff} values for 0.02 meV $< E <$ 0.08 meV. After that, the values increased suddenly at 0.1 meV (PE dominant) then starts to reduce radically up to 0.8 meV, which become the values almost constant up to 3 meV. Above this energy level, the Z_{eff} starts increasing softly up to 10 meV. Finally, the addition of K_2O, Na_2O, CaO, SrO and BaO enhances the Z_{eff} and this is expected since the atomic number of elements are higher than B. The effective electron density (N_{eff}) is also determined for the new prepared glasses as shown in Fig. 14. The values were measured at various energies (0.01 up to 10 meV) showed the same pattern obtained in Z_{eff} curves. The maximum N_{eff} is found at low energy and the minimum values occurred above 3 meV. The variation in these values ascribed to the possibility of photon cross section in the absorber (photoelectron, Compton scattering and pair production) as we mentioned in the previous paragraph.

The SAFE is referred to the specific absorbed fraction of the energy (the portion of energy emitted by a specific source and absorbed per unit mass of absorber). In this study, we measured the SAFE up to 40 mfp at a 0.001 cm thickness for the highest μ_m (BPBBaE) shown in Fig. 15. The obtained results show a gradual reduction in the SAFE values up to (0.15 meV), after that the SAFE values start to increase up to 0.8 meV. The Compton scattering at this energy (intermediate range) exceeds and radiation scattering increased and be dominant compared to the absorption effect. The minimum SAFE values noticed at high energies in which the pair production is dominant and the possibility of specific absorption reduced [50]. Another significant particle for radiation shielding concerning the particulate radiation emission is the total stopping power (TSP). In the current study, the prepared glasses for electron were determined by using the ESTAR program [51–53] as shown in Fig. 16. The maximum TSP values of

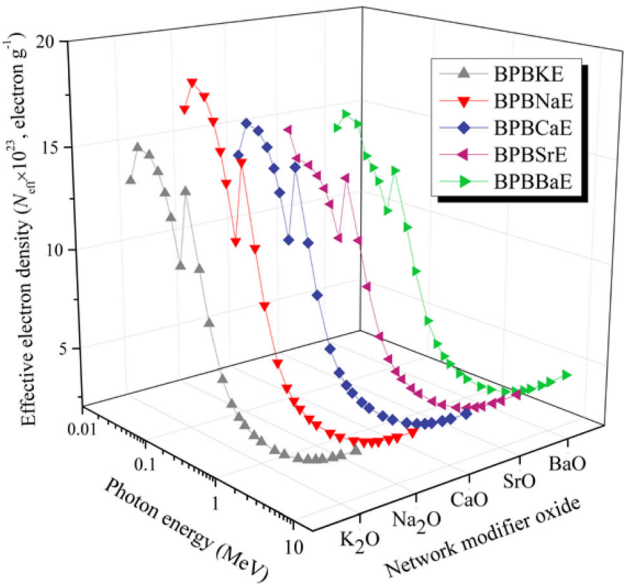

Fig. 14 Variation of the effective electron density number (N_{eff}) with photon energy for new glasses

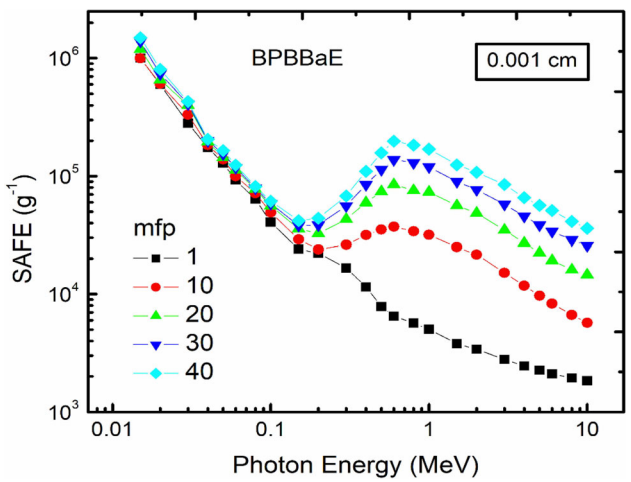

Fig. 15 The variation of SAFE with incident photon energy for BPBBaE at 0.001 cm at various mfps

electron was reported at low energy and start to reduce with high rate with increasing incident kinetic energy (up 1 meV), and above this energy level (> 1 meV) the TSP values become almost constant. The slightly increase in the high energy level (> 3 meV) is referred to the pair production probability at this level. The sample with the highest μ_m (BPBBaE) revealed the lowest values of electron TSP. Furthermore, calculating continuous slowing down approximation range (CSDA) is one of the convenient ways to estimate the electron stopping in different absorber. This parameter gives an approximate

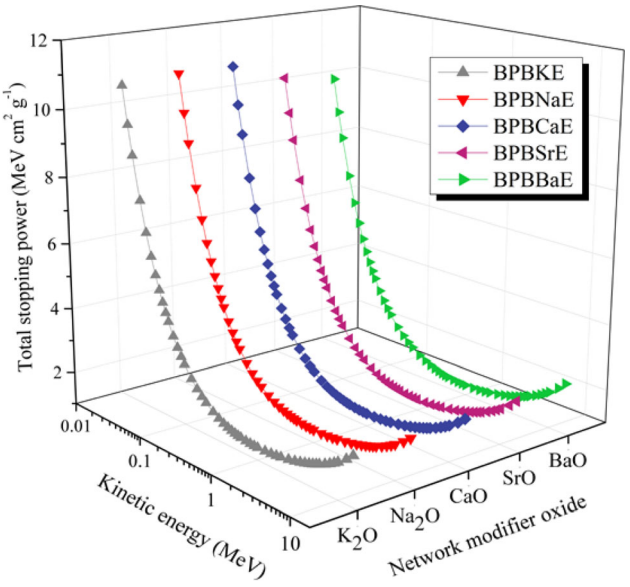

Fig. 16 Variation of mass stooping power (for electron emission) with photon energy for new glasses

average about the path length of traveling electrons before absorption. The direct relation between CSDA and kinetic energy released by electron is expected as we shown in Fig. 17. The highest CSDA values in the new glasses were reported at 10 meV. Finally, similar findings of TSP and CSDA parameters were reported for different glasses elsewhere [54–57].

4 Conclusion

In summary, Eu^{3+} ions doped Bismuth Lead borate glasses are synthesized by melt quenching technique and following results are observed;

1. From the XRD analysis, the glass is found to be in amorphous nature since there are no significant peaks to denote the crystalline nature of the sample.
2. Densities and refractive indices increases when one move from BPBKE to BPBBaE glasses.
3. From structural studies, it is found that the glasses have high connectivity with large number of bridging oxygens and so the glass has more rigid network.
4. From optical studies, the transition $^7F_0 \rightarrow {}^5D_2$ is termed as hypersensitive transition since it obeys the selection rules $\Delta J \leq 2$ and $\Delta L \leq 2$. Band gap increases with the increase in the density of glasses and Urbach energy values gives the

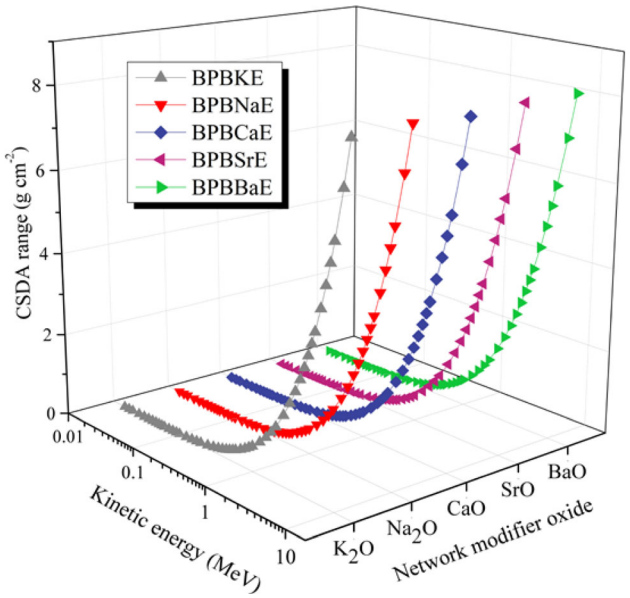

Fig. 17 Variation of continuous slowing down approximation (CSDA) with photon energy for new glasses

results that the glasses possess very less disorderliness.

5. The smallest HVL is achieved with BPBBaE glass. Such that at 0.1 meV the HVL is varied between 0.0711 cm (for BPBKE), 0.0691 cm (for BPBNaE), 0.0587 (for BPBCaE), 0.0505 (for BPBSrE) and 0.0404 (for BPBBaE).
6. The obtained results show a gradual reduction in the SAFE values up to (0.15 meV) and then start to increase up to 0.8 meV.
7. The maximum TSP values of electron was reported at low energy and start to reduce with high rate with increasing incident kinetic energy (up 1 meV), and above this energy level (> 1 meV) the TSP values become almost constant.

Compliance with ethical standards

Conflict of interest We have no conflict of interest to declare.

References

1. Y. Al-Hadeethi, M.I. Sayyed, J. Kaewkhao, A. Askin, B.M. Raffah, E.M. Mkawi, R. Rajaramakrishna, Appl. Phys. A. **125**, 852 (2019)
2. M.I. Sayyed, J. Alloys Compd. (2016). https://doi.org/10.1016/j.jallcom.2016.07.153
3. M. Almatari, O. Agar, E.E. Altunsoy, O. Kilicoglu, M.I. Sayyed, H.O. Tekin, Results Phys. (2019). https://doi.org/10.1016/j.rinp.2019.01.094
4. E. Kavaz, H.O. Tekin, O. Agar, E.E. Altunsoy, O. Kilicoglu, M. Kamislioglu, M.M. Abuzaid, M.I. Sayyed, Ceram. Int. (2019). https://doi.org/10.1016/j.ceramint.2019.05.028
5. F. Laariedh, M.I. Sayyed, A. Kumar, H.O. Tekin, R. Kaur, T.B. Badeche, J. Non-Cryst. Solids (2019). https://doi.org/10.1016/j.jnoncrysol.2019.03.007
6. K.M. Kaky, M.I. Sayyed, A. Khammas, A. Kumar, E. Şakar, A.H. Abdalsalam, B.C. Şakar, B. Alim, M.H. Mhareb, Mater. Chem. Phys. (2020). https://doi.org/10.1016/j.matchemphys.2019.122504
7. N. Singh, K.J. Singh, K. Singh, H. Singh, Nucl. Instrum. Methods Phys. Res. Sect. B (2004). https://doi.org/10.1016/j.nimb.2004.05.016
8. M.A. Marzouk, F.H. ElBatal, W.H. Eisa, N.A. Ghoneim, J. Non-Cryst Solids (2014). https://doi.org/10.1016/j.jnoncrysol.2014.01.002
9. M. Wilson, Mater. Chem. Phys. (2019). https://doi.org/10.1016/j.matchemphys.2018.12.022
10. L.Q. Yao, G.H. Chen, T. Yang, S.C. Cui, Z.C. Li, Y. Yang, Ceram. Int. (2016). https://doi.org/10.1016/j.ceramint.2016.05.092
11. A. Wagh, Y. Raviprakash, S.D. Kamath, J. Alloys Compd. (2017). https://doi.org/10.1016/j.jallcom.2016.11.299
12. V. Hegde, N. Chauhan, V. Kumar, C.D. Viswanath, K.K. Mahato, S.D. Kamath, J. Lumin. (2019). https://doi.org/10.1016/j.jlumin.2018.11.023
13. L.Q. Yao, G.H. Chen, S.C. Cui, H.J. Zhong, C. Wen, J. Non-Cryst. Solids (2016). https://doi.org/10.1016/j.jnoncrysol.2016.04.039
14. H.H. Hegazy, M.S. Al-Buriahi, F. Alresheedi, F.I. El-Agawany, C. Sriwunkum, R. Neffati, Y.S. Rammah, Ceram. Int. (2020). https://doi.org/10.1016/j.ceramint.2020.09.131
15. V.P. Singh, N.M. Badiger, J. Kaewkhao, J. Non-Cryst. Solids (2014). https://doi.org/10.1016/j.jnoncrysol.2014.08.003
16. Y. Chen, G. Chen, X. Liu, J. Xu, T. Yang, C. Yuan, C. Zhou, J. Non-Cryst. Solids (2018). https://doi.org/10.1016/j.jnoncrysol.2018.01.027
17. G. Sathiyapriya, K. Marimuthu, M.I. Sayyed, A. Askin, O. Agar, J. Non-Cryst. Solids (2019). https://doi.org/10.1016/j.jnoncrysol.2019.119574
18. S.A. Issa, H.O. Tekin, R. Elsaman, O. Kilicoglu, Y.B. Saddeek, M.I. Sayyed, Mater. Chem. Phys. (2019). https://doi.org/10.1016/j.matchemphys.2018.10.064

19. B. Opers, T. Radu, S. Simon, J. Non-Cryst. Solids (2013). https://doi.org/10.1016/j.jnoncrysol.2013.07.024
20. H.S. Liu, T.S. Chin, S.W. Yung, Mater. Chem. Phys. (1997). https://doi.org/10.1016/S0254-0584(97)80175-7
21. J.A. Jiménez, E.R. Fachini, C. Zhao, J. Mol. Struct. (2018). https://doi.org/10.1016/j.molstruc.2018.03.095
22. A. Majjane, A. Chahine, M. Et-tabirou, B. Echchahed, T.O. Do, P. Mc Breen, Mater. Chem. Phys. (2014). https://doi.org/10.1016/j.matchemphys.2013.10.013
23. M.J. Berger, J.H. Hubbell, XCOM: photon cross sections on a personal computer. NBSIR **87**, 3597 (1987). https://doi.org/10.2172/6016002
24. D.F. Swinehart, J. Chem. Educ. (1962). https://doi.org/10.1021/ed039p333
25. P. Kaur, K.J. Singh, M. Kurudirek, S. Thakur, Spectrochim. Acta A (2019). https://doi.org/10.1016/j.saa.2019.117309
26. V. Dimitrov, S. Sakka, J. Appl. Phys. (1996). https://doi.org/10.1063/1.360963
27. A.S. Abouhaswa, M.H. Mhareb, A. Alalawi, M.S. Al-Buriahi, J. Non-Cryst. Solids (2019). https://doi.org/10.1016/j.jnoncrysol.2020.120130
28. D.K. Gaikwad, M.I. Sayyed, S.N. Botewad, S.S. Obaid, Z.Y. Khattari, U.P. Gawai, F. Afaneh, M.D. Shirshat, P.P. Pawar, J. Non-Cryst. Solids (2019). https://doi.org/10.1016/j.jnoncrysol.2018.09.038
29. M. Mariyappan, K. Marimuthu, M.I. Sayyed, M.G. Dong, U. Kara, J. Non-Cryst. Solids (2018). https://doi.org/10.1016/j.jnoncrysol.2018.07.025
30 R. Divina, K. Marimuthu, M.I. Sayyed, H.O. Tekin, O. Agar, Radiat. Phys. Chem. (2019). https://doi.org/10.1016/j.radphyschem.2019.03.029
31 M.K. Halimah, M.N.A. Hazlin, F.D. Muhammad, Spectrochim. Acta A (2018). https://doi.org/10.1016/j.saa.2017.12.054
32. I.Z. Hager, R. El-Mallawany, J. Mater. Sci. (2010). https://doi.org/10.1007/s10853-009-4017-3
33. H. Jabraoui, M. Badawi, S. Lebègue, Y. Vaills, J. Non-Cryst. Solids (2018). https://doi.org/10.1016/j.jnoncrysol.2018.07.004
34 A. Abd El-Moneim, J. Fluorine Chem. (2019). https://doi.org/10.1016/j.jfluchem.2019.03.007
35. K. Annapoorani, K. Marimuthu, J. Non-Cryst. Solids (2017). https://doi.org/10.1016/j.jnoncrysol.2017.03.004
36. L. Xia, L. Wang, Q. Xiao, Z. Li, W. You, Q. Zhang, J. Non-Cryst. Solids (2017). https://doi.org/10.1016/j.jnoncrysol.2017.09.049
37 R. Vijayakumar, K. Maheshvaran, V. Sudarsan, K. Marimuthu, J. Lumin. (2014). https://doi.org/10.1016/j.jlumin.2014.04.022
38. R. Rajaramakrishna, P. Nijapai, P. Kidkhunthod, H.J. Kim, J. Kaewkhao, Y. Ruangtaweep, J. Alloys Compd. (2020). https://doi.org/10.1016/j.jallcom.2019.151914
39. Berger, M.J., Hubbell, J.H.: XCOM: photon cross sections on a personal computer. No. NBSIR-87-3597. National Bureau of Standards, Washington, DC (USA). Center for Radiation Research (1987)
40. Y.S. Alajerami, D. Drabold, M.H. Mhareb, K.L. Cimatu, G. Chen, M. Kurudirek, Ceram. Int. (2020). https://doi.org/10.1016/j.ceramint.2020.02.039
41. Y.S. Alajerami, D.A. Drabold, M.H. Mhareb, K.N. Subedi, K.L. Cimatu, G. Chen, J. Appl. Phys. (2020). https://doi.org/10.1063/1.5143116
42. M.S. Al-Buriahi, M.I. Sayyed, Y. Al-Hadeethi, Ceram. Int. (2020). https://doi.org/10.1016/j.ceramint.2020.02.148
43. M.G. Dong, X.X. Xue, Y. Elmahroug, M.I. Sayyed, M.H.M. Zaid, Results Phys. (2019). https://doi.org/10.1016/j.rinp.2019.02.065
44. J. Allison, K. Amako, J. Apostolakis, P. Arce, M. Asai, T. Aso, E. Bagli, A. Bagulya, S. Banerjee, G. Barrand, B.R. Beck, A.G. Bogdanov, D. Brandt, J.M.C. Brown, H. Burkhadt, P. Canal, D. Cano-Ott, S. Chauvie, K. Cho et al., Nucl. Instrum. Methods Phys. Res. Sect. A (2016). https://doi.org/10.1016/j.nima.2016.06.125
45. SCHOTT: https://www.schott.com/advanced_optics/english/products/opticalmaterials/ special-materials/radiation-shielding-glasses/index.html. Accessed 03 Sept 2018
46. I.I. Bashter, Ann. Nucl. Energy (1997). https://doi.org/10.1016/S0306-4549(97)00003-0
47. S.R. Manohara, S.M. Hanagodimath, K.S. Thind, L. Gerward, Nucl. Instrum. Methods B (2008). https://doi.org/10.1016/j.nimb.2008.06.034
48. K.A. Naseer, K. Marimuthu, M.S. Al-Buriahi, A. Alalawi, H.O. Tekin, Ceram. Int. (2020). https://doi.org/10.1016/j.ceramint.2020.08.138
49. I. Boukhris, A. Alalawi, M.S. Al-Buriahi, I. Kebaili, M.I. Sayyed, Ceram. Int. (2020). https://doi.org/10.1016/j.ceramint.2020.05.047
50. M.S. Al-Buriahi, V.P. Singh, A. Alalawi, C. Sriwunkum, B.T. Tonguc, Ceram. Int. (2020). https://doi.org/10.1016/j.ceramint.2020.03.091
51. Y.B. Saddeek, S.A. Issa, T. Alharbi, K. Aly, M. Ahmad, H.O. Tekin, Ceram. Int. (2020). https://doi.org/10.1016/j.ceramint.2019.09.254
52. J.F. Ziegler, M.D. Ziegler, J.P. Biersack, Nucl. Instrum. Methods B (2010). https://doi.org/10.1016/j.nimb.2010.02.091
53. The Stopping and Range of Ions in Matter (SRIM) www.srim.org.

54. I.O. Olarinoye, Y.S. Rammah, S. Alraddadi, C. Sriwunkum, A.F. Abd El-Rehim, H.Y. Zahran, M.S. Al-Buriahi, Ceram. Int. (2020). https://doi.org/10.1016/j.ceramint.2020.08.092
55. I. Boukhris, I. Kebaili, M.S. Al-Buriahi, A. Alalawi, A.S. Abouhaswa, B. Tonguc, Ceram. Int. (2020). https://doi.org/10.1016/j.ceramint.2020.06.226
56. M.S. Al-Buriahi, E.M. Bakhsh, B. Tonguc, S.B. Khan, Ceram. Int. (2020). https://doi.org/10.1016/j.ceramint.2020.04.240
57. I. Kebaili, I. Boukhris, M.S. Al-Buriahi, A. Alalawi, M.I. Sayyed, Ceram. Int. (2020). https://doi.org/10.1016/j.ceramint.2020.08.251